Bio-Design and Manufacturing (2023) 6:691–703
https://doi.org/10.1007/s42242-023-00253-3

RESEARCH ARTICLE

Rapid printing of 3D porous scaffolds for breast reconstruction

Pengcheng Zhao[1,2] · Biling Wang[1] · Lu Wang[2] · Zexin Fu[2] · Jun Hu[1] · Yande Liu[1] · Ji Wang[2] · Yong He[3]

Received: 14 February 2023 / Accepted: 20 June 2023 / Published online: 14 October 2023

Abstract

Prosthesis implantation and fat transplantation are common breast reconstruction methods. In general, prosthesis implantation alone does not achieve a realistic enough appearance, and fat transplantation alone is difficult to achieve in the correct capacity. To date, no reports have focused on methods of combining fat with implanted prostheses for breast reconstruction. Using a newly designed bionic ink (i.e., polyether F127 diacrylate (F127DA) & poly(ethylene glycol) diacrylate (PEGDA)) and projection-based three-dimensional bioprinting (PBP), we report the development of a new method for printing porous prostheses. PEGDA was used to improve the printing precision of the prosthesis by increasing the gel point of F127DA and reducing the impact of external temperature. The compression modulus of the printed prosthesis was very close to that of prostheses currently used in clinical practice and to that of natural breasts. Finally, stromal vascular fraction gel (SVF-gel), a human fat extract, was injected into the pores of the synthesized prostheses to prepare a prosthesis mixed with adipose tissue. These were implanted subcutaneously in nude mice to observe their biological performance. After 14 and 28 days of observation, the prosthesis showed good biocompatibility, and adipose tissues grew well in and around the prosthesis. This result shows that a porous prosthesis containing pre-placed adipose tissues is a promising breast reconstruction material.

✉ Yande Liu
jxliuyd@163.com

✉ Ji Wang
jiwang1004@zju.edu.cn

✉ Yong He
yongqin@zju.edu.cn

[1] School of Mechatronics and Vehicle Engineering, East China Jiaotong University, Nanchang 330013, China

[2] Center for Plastic and Reconstructive Surgery, Department of Plastic and Reconstructive Surgery, Zhejiang Provincial People's Hospital (Affiliated People's Hospital, Hangzhou Medical College), Hangzhou 310014, China

[3] Key Laboratory of 3D Printing Process and Equipment of Zhejiang Province, School of Mechanical Engineering, Zhejiang University, Hangzhou 310027, China

Graphic abstract

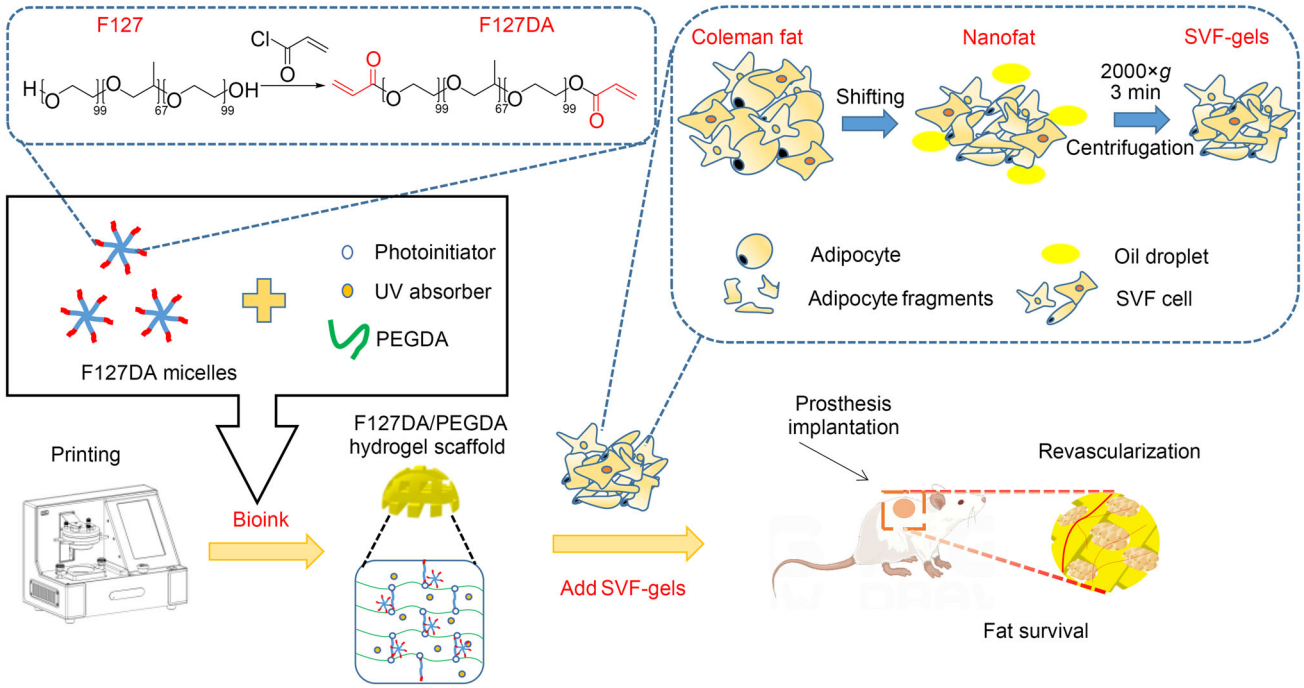

Keywords Projection-based 3D bioprinting (PBP) · F127DA · Breast reconstruction · Fat transplantation

Introduction

Worldwide, breast cancer is the most common cancer among women, and accounts for one-third of all female cancers [1–3]. Most breast cancer patients undergo total mastectomy, which may cause anxiety and depression [4]. As an important field of plastic surgery, breast reconstruction has been proven to improve the psychological, physical, and sexual health of women with breast defects [5]. Since the beginning of the twenty-first century, autologous fat filling has been increasingly used as a method of breast reconstruction [6–8]. At present, the main methods of breast reconstruction after mastectomy are autologous tissue interventions and prosthesis reconstructions. In many parts of the world, breast reconstruction using autologous tissue is the gold standard, since it uses autologous skin and fat to replace the breast tissue [9]. Fat filling is a common method for breast reconstruction, but 70% of fat is generally lost due to fat necrosis and autoabsorption [10]. Moreover, even the improved Coleman fat filling method results in 20%–30% fat loss [11, 12]. The use of nanofat improves these properties, and nanofat filling has been shown to result in higher fat retention, better tissue structures, and improved capillary density [13, 14]. However, the presence of oil droplets and fat necrosis can lead to chronic inflammation [15]. Stromal vascular fraction (SVF) gel is fat treated with a nanofat degreaser, and has shown higher survival rates and better biocompatibility [16]. In summary, autologous fat filling requires large amounts of fat, and its high mobility makes breast shaping relatively difficult, which requires surgeons with extensive experience.

Another method of breast reconstruction is prosthesis reconstruction, which has better shaping ability and customizability than methods using autologous fat. At present, silicone prostheses are the most commonly used. However, after implantation, they may cause chronic inflammation conditions such as capsular contracture and granuloma, which can result in the formation of cysts and fibrosis [17, 18]. In recent years, three-dimensional (3D) printing [19, 20] has provided a new protocol for breast reconstruction. Many researchers have obtained breast models via magnetic resonance imaging and then developed prostheses through 3D printing [21]. Some researchers have also made prostheses using novel modeling and printing methodologies. For example, Tytgat et al. [22] used an extrusion printing method to manufacture breast prostheses that showed good biocompatibility, mechanical properties similar to those of a natural breast, and a limited ability to promote fat. Shi et al. [23] also used extrusion printing to produce scaffolds with hemostatic function and good pH sensitivity. However, these 3D-printing

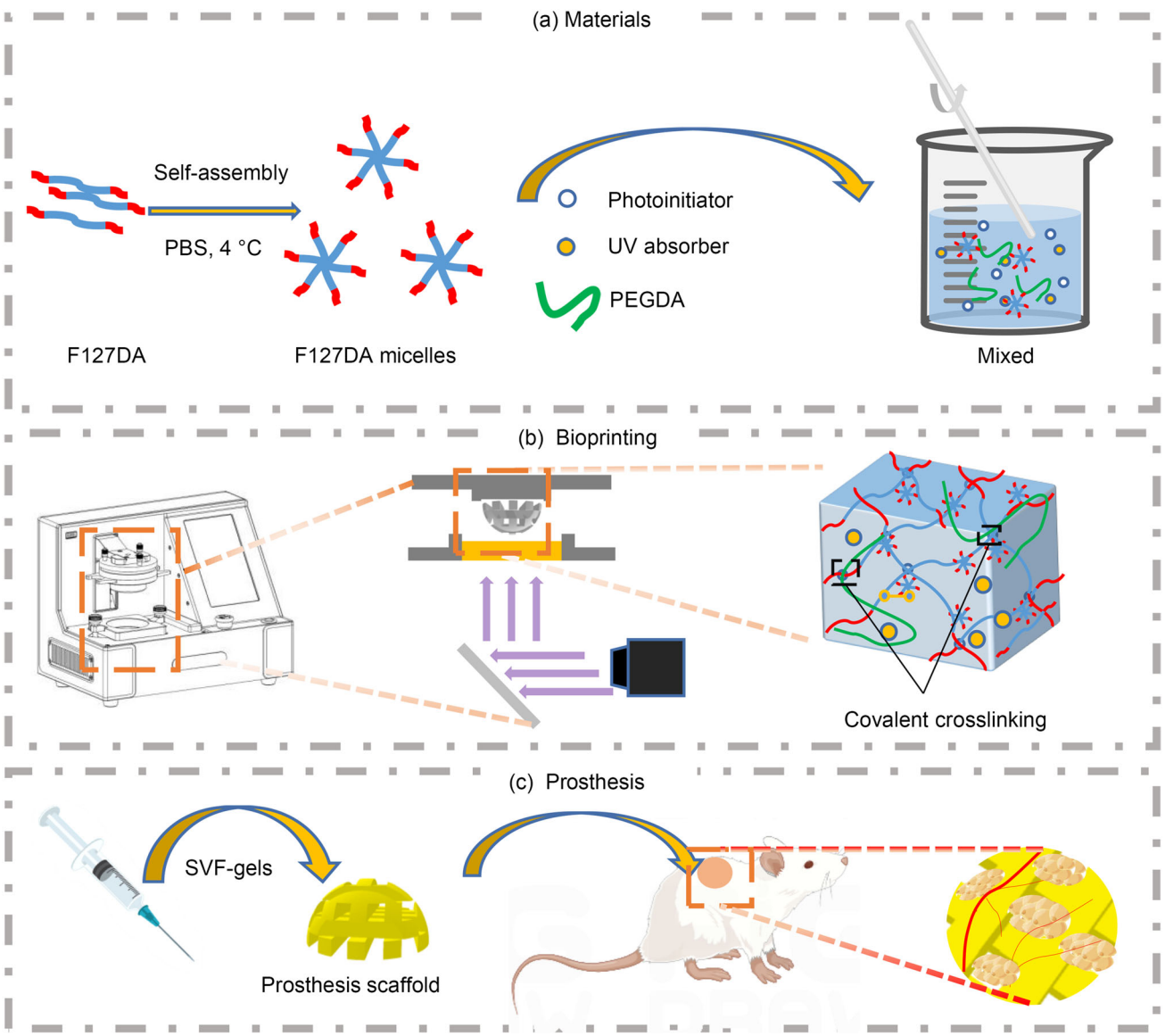

Fig. 1 F127DA & PEGDA prosthetic scaffold. **a** Preparation of bioink. **b** Bioprinting: a schematic representation of PBP and gelling. **c** Prosthesis: the prosthetic stent was filled with SVF-gels and implanted into the body. After 14 and 28 days, the internal tissue structure was removed and observed. F127DA: polyether F127 diacrylate; PEGDA: poly(ethylene glycol) diacrylate; PBP: projection-based 3D bioprinting; SVF: stromal vascular fraction

prosthetic reconstruction methods rely heavily on biological materials.

In this study, we developed a bioink that also shows high biocompatibility, and we therefore proposed a new breast reconstruction method (Fig. 1). The prosthesis manufactured using the projection-based 3D bioprinting (PBP) process shows good biocompatibility and a compression modulus similar to that of the natural breast. Moreover , it does not quickly degrade, i.e., it has a good shaping effect. We combined the autologous fat transplantation and prosthesis reconstruction protocols by implanting a printed porous breast prosthesis with an SVF-gel into nude mice and observed the results. The final results showed that we achieved a satisfactory breast reconstruction. We believe that these results will help develop more effective methods of breast reconstruction.

Materials and methods

Materials

F127 (molecular weight 1.5×10^4 Da) was obtained from Sigma (USA); lithium phenyl(2,4,6-trimethylbenzoyl)phosphinate (LAP), tartrazine, and potassium carbonate were obtained from Shanghai Aladdin Biochemical Co., Ltd. (China); acryloyl chloride, dichloromethane (DCM), and poly(ethylene glycol) diacrylate (PEGDA, molecular weight 600 Da) were obtained from Shanghai Macklin Biochemical Co., Ltd. (China); Dulbecco's modified Eagle medium (DMEM), fetal bovine serum, double antibody, trypsin, and 1× cell culture grade phosphate-buffered saline (PBS) were obtained from Dalian Meilun Biotechnology Co., Ltd. (China).

Preparation of polyether F127 diacrylate (F127DA)

The preparation of F127DA was performed using an improved version of a previously published protocol [24–26]. Briefly, we first dried a reaction flask for 24 h, after which pluronic F127 was added and dissolved in DCM. Next, an appropriate amount of acryloyl chloride was added, after which an amount of potassium carbonate was added to promote the reaction. The resulting mixture was then stirred at 15 °C for 50 h. After the reaction, impurities were removed using an RE100 Pro digital display rotary evaporator (Beijing Dragon-DLAB, China) and a filter screen with a retention rate of 6000 Da. Finally, after impurity removal, the solution was freeze-dried for 24 h to obtain a relatively pure F127DA powder.

Determination of the degree of acryloylation

Next, we used ^{1}H-NMR (NMR, nuclear magnetic resonance; 400 MHz) to determine the degree of substitution of F127DA. We then dissolved a polymer sample at a specified concentration in deuterated water to prepare 1% F127DA and 1% F127 solutions for NMR measurement. All chemical shifts for resonance peaks were reported in parts per million (ppm). The obtained nuclear magnetic hydrogen spectrum was analyzed using MestReNova (Mestrelab Research SL, Spain).

All ^{1}H-NMR spectra were recorded using a zg30 pulse sequence on a Bruker 600 MHz AVANCE III spectrometer equipped with a 5 mm broad band fluorine observation (BBFO) probe at 25 °C. Swimming and proton pulse calibrations were performed automatically for each sample before data acquisition. All data were then processed using Bruker Topspin 3.2. The spectral width was 20 MHz and the number of scans was 128.

Rheological properties

An AntonPaar MCR 301e (AntonPaar, Shanghai, China) rheometer equipped with semiconductor refrigeration chips, a thermostatic system, and a portable ultraviolet (UV) source (OmniCurve S2000 Spot UV Curing System, 405 nm wavelength, 18 mW/cm^2) was used for all rheological tests. For the viscosity experiment, the shear rate was held constant at 10 s^{-1}. The viscosity of 15% (0.15 g/mL) F127DA with different concentrations of PEGDA was measured at 4 °C and 25 °C. A 650-μL sample was taken on the measuring platform and measured after the temperature had stabilized.

For the temperature gel (temperature-sensitive) experiment, oscillating measurement was carried out under a strain frequency of 2 rads^{-1} and 1% strain. The sample was first equilibrated at 4 °C for 5 min and then heated from 4 to 40 °C at a rate of 5 °C/min. The intersection of the storage modulus *G*' and the loss modulus *G*" was taken as the gel temperature.

For the photocrosslinking experiment, oscillating measurements were made at a strain frequency of 5 rads^{-1} and 1% strain. A 650-μL sample was taken and equilibrated at 25 °C for 5 min on the measuring platform, after which the program was run. After 30 s, the UV light source was turned on for UV crosslinking, and the maximum intensity was 90% (18 mW/cm^2). All measurements were repeated three times to ensure consistency.

3D printing

The printer used in the experiment was a projection photocuring biological 3D printer (EFL-BP8601Pro, Suzhou Yongqinquan Intelligent Equipment Co., Ltd., Suzhou, China) equipped with a 405 nm UV source, a thermostatic system, and a 25 μm high-precision digital micromirror device (DMD) chip. First, a hydrogel precursor solution was prepared, which contained 15% F127DA, 3% (0.03 g/mL) PEGDA, 0.25% (2.5 g/L) LAP, and an appropriate content of tartrazine. Second, the STL model of the prosthetic scaffold was imported into the software controller of the EFL-BP8601Pro printer to compute the slicing profile. The height of each layer was 100 μm. Third, we set the printer's light intensity to 18 mW/cm^2 and its exposure time to 6–8 s. The scaffold was a hemispherical porous structure with a height of 5 mm and a diameter of 10 mm. The pore size of the designed scaffold was 1 mm × 1 mm, and the theoretical porosity of the designed scaffold, as calculated using Python, was 49.56%.

Compression performance

We used a Sansi Zongheng UTM2000 series electronic universal testing machine (Shenzhen Sansi Zongheng Technology Co., Ltd., Shenzhen, China) to obtain the compression curve of the hydrogel [27]. We then used the machine to test

the compression modulus of the breast prosthesis scaffold as well as that of a commercial prosthesis [28, 29]. This was done by compressing each at a rate of 0.5 mm/min until it reached 70% of its initial height; we therefore obtained the compression curve of each prosthesis. The compression modulus of the prosthesis was calculated using its linear region (i.e., the first 10%).

In vitro experiments

Swelling ratio

To prepare samples for swelling analysis, the bioink was placed in a transparent cylinder container (5 mm in diameter) and photocrosslinked. When the photopolymerization had completed, we used PBS to wash away materials whose surfaces had not completely cured. Next, the hydrogel block was placed in a centrifuge tube containing 2 mL PBS. Excess water was then gently removed using a paper tissue and the weight of the swollen hydrogel block was measured using a precision balance. The swelling ratio was defined as follows:

$$\text{swelling ratio} = \frac{W_s - W_0}{W_0} \times 100\%,$$

where W_s is the swollen weight of the sample and W_0 is the dry weight of the sample. Each hydrogel component was measured for seven days using three replicates.

Cell culture

Human umbilical vein endothelial cells (HUVECs, Nanjing Saihongrui Biotechnology Co., Ltd., Nanjing, China) were first cultured in DMEM containing 4.5 g/L glucose, to which 10% fetal bovine serum and 1% penicillin/streptomycin were added. Cells were kept at 37 °C and 5% carbon dioxide and were subcultured every two days [30].

Cell cytotoxicity assay

For qualitative observation of the co-culturing of cells with the hydrogel, a live/dead cell staining kit (KeyGEN BioTECH, Jiangsu Keygen Biotech Co., Ltd., China) was used to detect the effects of the solidified hydrogel on cell viability after adding different concentrations of PEGDA. To measure the cell viability, living cells were stained green and imaged using a fluorescence microscope. Cells were then counted and resuspended at 2×10^4 cells/mL. HUVECs were cultured in 96-well plates at 37 °C in a 5% carbon dioxide atmosphere. Next, the HUVECs were co-cultured with the cured F127DA, F127DA@3%PEGDA (F127DA added with 3% PEGDA), F127DA@5%PEGDA (F127DA added with 5% PEGDA), and F127DA@8%PEGDA (F127DA added with 8% PEGDA) hydrogels for periods of 0, 24, and 48 h. A culture of HUVECs without a hydrogel was used as a blank group. Finally, cells were stained with live/dead cell dyes for 20 min and their morphologies were observed by fluorescence microscopy. Cell counting was then performed using ImageJ.

Quantitative observation

Cytotoxicity and cell proliferation were measured at different time points (i.e., 0, 24, and 48 h) using cell counting kit-8 (CCK-8, Beyotime, Shanghai, China). Briefly, 50 μL CCK-8 solution and 500 μL fresh medium were added to each well of a multi-well plate and incubated for 2 h. The mixed solution was then transferred to 96-well plates in the dark, and the absorbance was measured using a microplate reader (Infinite F50, TECAN, Switzerland) at a wavelength of 450 nm [31].

In vivo experiments

Prosthesis implantation

Three eight-week-old female thymus-free nude mice (Shanghai SLAC Laboratory Animal Co., Ltd., Shanghai, China) were used for animal experiments. These mice were raised in a standardized pathogen-free animal room, in which they could freely obtain standard food and water. The room was maintained with a light/dark cycle at a stable temperature for 12 h. All surgical operations were performed under anesthesia with 2% isoflurane inhalation, and all procedures were performed by the same person as follows. First, a midline incision of 1 cm in length was made to the dorsal skin along the spine of each mouse. Next, the sterilized scaffold was implanted under the skin, and 100 μL aliquots of SVF-gels were injected [32]. The incision was closed using 6–0 silk thread via interrupted suture and was sterilized with 1% iodine. In addition, we subcutaneously injected 100 μL fat tissue into one of the mice as a no-scaffold control to observe whether the grafted fat would survive without a scaffold. We then closed and sterilized all incisions. Each animal was checked every two days to observe the occurrence of abnormal events during treatment.

This experiment was conducted in accordance with the guidelines of the Ethics Committee of Zhejiang Provincial People's Hospital. The adipose tissue used was fat tissue discarded from plastic surgery liposuction procedures performed at Zhejiang Provincial People's Hospital. The study protocol obtained an informed consent exemption and all procedures were approved by the Ethics Committee of Zhejiang Provincial People's Hospital, Hangzhou, China.The approval number is QT2022382.

Histological analysis

We used hematoxylin-eosin (HE) staining to observe the morphology and survival of the adipose tissue. To do so, samples were first dehydrated using a graded ethanol series and then embedded in paraffin. Wax blocks were then cut into 3–4-mm-thick slices. Next, all sections were dewaxed using xylene, rehydrated using a high-to-low concentration ethanol series, placed in distilled water, stained with HE, and finally observed under a light microscope.

Statistical analysis

All data are expressed as mean±standard deviation. Each independent test was repeated at least three times, and parallel tests were used to ensure effectiveness. We used GraphPad Prism version 8.3 (GraphPad Software Company, USA) for statistical analyses. Single-factor analysis of variance was used to determine the statistical significance of differences among group means. These were followed by multiple comparison tests. Finally, independent *t*-tests were performed to compare pairwise differences between group means. Statistical significance was considered when $P<0.05$.

Results and discussion

Preparation of materials

In the past, triethylamine was used as the positive reaction condition for F127DA synthesis. However, in this study we used potassium carbonate instead of triethylamine, and F127 was directly synthesized with acryloyl chloride in the presence of potassium carbonate (Fig. 2a). Synthesis of F127DA can occur with different degrees of substitution according to the material ratio of acryloyl chloride to F127 present in the reaction mixture. Next, we used ^{1}H-NMR spectra [33] to compare the relative peak ratios of methylene protons (=CH_2, 5.8–6.4 ppm) in acrylate and methyl protons (–CH_3, 1–1.2 ppm) on the side chain of F127DA; we found that the degree of substitution was approximately 90% (Fig. 2b).

F127DA is known to show excellent flexibility, elasticity, and toughness. It can be bent, knotted, compressed, or stretched at will. Moreover, it then returns to its initial state after unloading (Fig. 2c). The acrylic hydrogel also showed excellent printing performance, and after PEGDA was added, it was capable of printing very fine structures (Fig. 2d).

Rheological characteristics

To better understand the rheological properties of the bioink reported here, we used a rheometer to test the viscosity, temperature sensitivity, and UV curing modulus of the ink solution. As shown in Figs. 3a and 3b, differences in the concentration of PEGDA showed little effect on the ink viscosity. At 4 °C, the viscosity of the ink was concentrated at approximately 25 mPa·s, while at 25 °C, it was concentrated at about 50 mPa·s (Table 1).

When 15% F127DA was printed at room temperature (25 °C), the ink easily underwent physical gelation, which was one of the main factors that led to a decline in printing accuracy. We therefore added different concentrations of PEGDA, which strongly increased the gel point temperature of the ink (Fig. 3c). At the same time, we also recorded the gel point of PEGDA & F127DA and its modulus of stable physical gelation at 40 °C (Table 2). We found that while the gel point temperature of 15% F127DA was 22.27 °C (i.e., <25 °C), the gel point temperature of the solution after the addition of PEGDA increased significantly, which was beneficial for printing at room temperature.

Finally, to determine the most suitable light intensity and exposure time for printing, we tested the rheological properties of the UV curable ink. To do so, we adjusted the light intensity of the 405 nm light source to 18 mW/cm^2. According to the time–modulus curve (Fig. 3d) obtained from this test, we determined that when the light source was turned off, the storage modulus of the hydrogel was relatively low. However, when the light source was turned on at 30 s, the storage modulus of the hydrogel started to increase sharply, and by 6–8 s of illumination, the storage modulus of the hydrogel had almost reached its peak. At this point, we believe that the hydrogel was completely cured. Therefore, when we set the parameters of the printer, the light intensity and exposure time were set to 18 mW/cm^2 and 6 s, respectively.

Printability

Since this hydrogel material can be used as a crosslinking agent [34] and its two ends have double bonds that facilitate photocuring, we used it directly as the test material. To test its printability, we first used a 15% F127DA & 3% PEGDA precursor solution as the biological ink for PBP. For this process, we used a 10 mL glass bottle to load a certain amount of ink. This was then irradiated using a 405 nm UV light source for a few seconds to ensure that the material was photocurable (Fig. 4a). Finally, using data measured by the rheometer, we set up the printer for printing. The hydrogel can also be printed without the addition of crosslinking agent. However, when printed at room temperature, we found that the bioink was greatly affected by temperature, which led to a decline in the overall accuracy of the printed prosthesis. Therefore, we added small amount of PEGDA to improve the printing accuracy. Interestingly, when we added 3% PEGDA for printing, we found that the prosthesis printed at room temperature

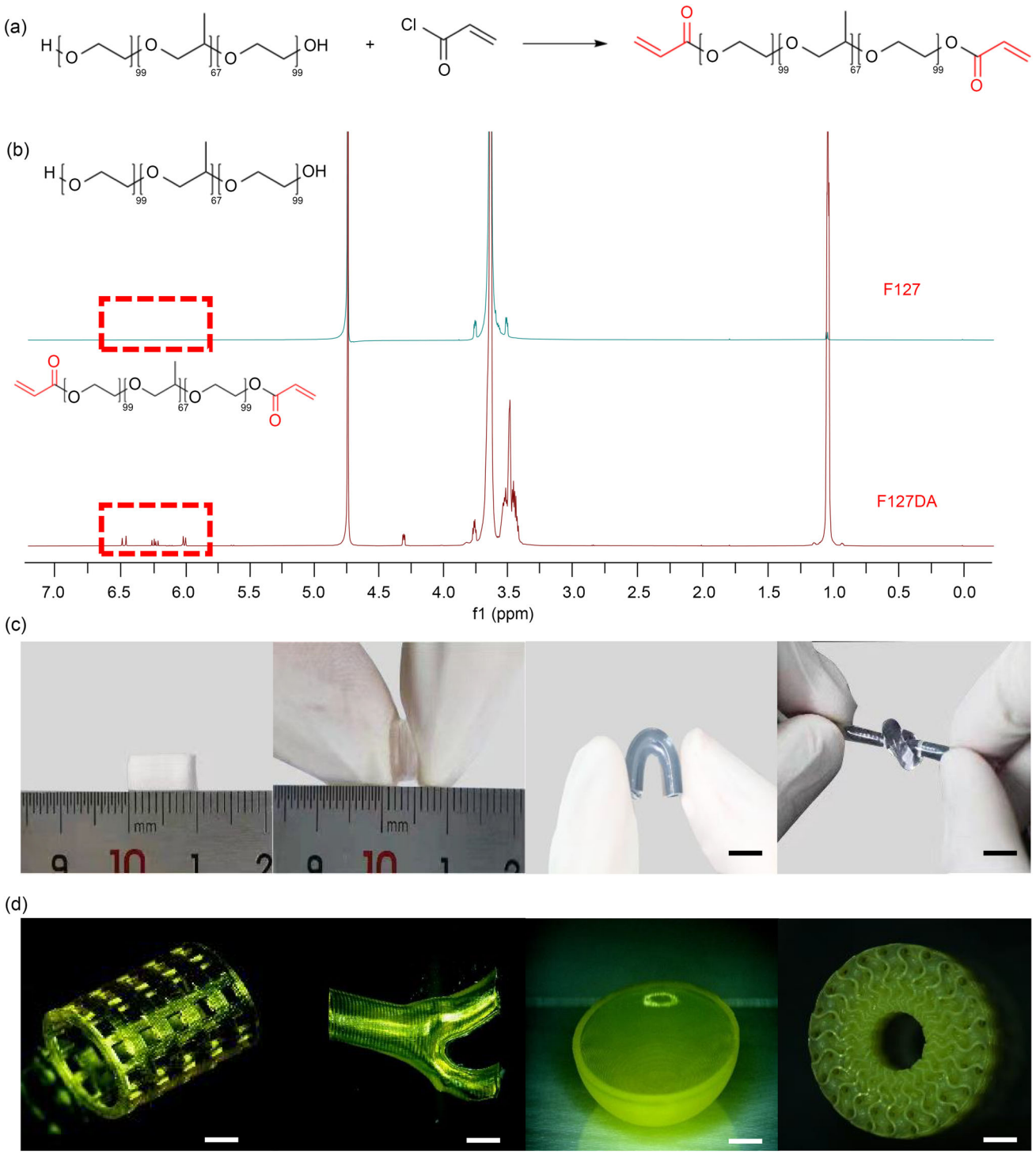

Fig. 2 The F127DA synthesis process. **a** F127 was acryloylated to obtain F127DA, which can be photocured. **b** Nuclear magnetic hydrogen spectra of F127 and F127DA. **c** F127DA is compressed, bent, and knotted after curing. Scale bar = 5 mm. **d** Images of the projection-based bioprinted complex structures. Scale bar=3 mm. F127DA: polyether F127 diacrylate

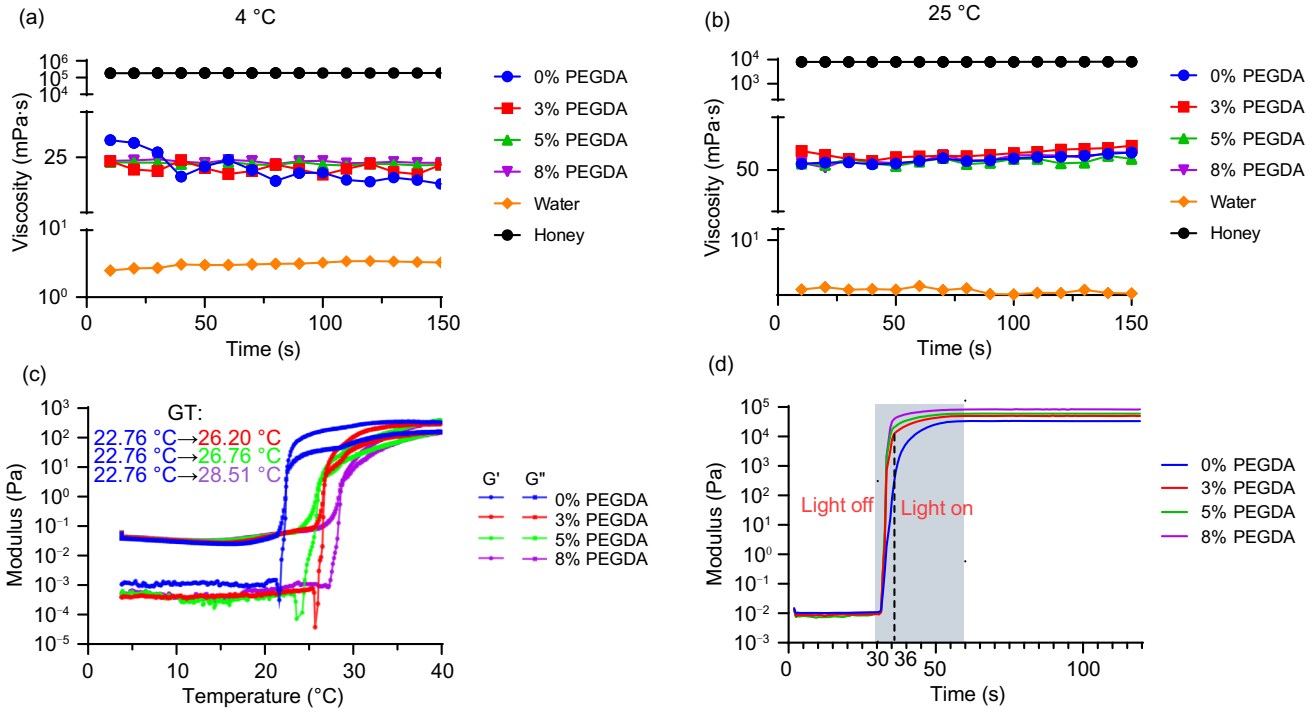

Fig. 3 Rheological properties. **a**, **b** Viscosity of 15% F127DA added with PEGDA of different concentrations at 4 °C and 25 °C, and the respective viscosities of water and honey at the corresponding temperatures. **c** The effect of different concentrations of PEGDA on the gelation temperature during heating from 4 to 40 °C. **d** Photocuring rheological test. F127DA: polyether F127 diacrylate; PEGDA: poly(ethylene glycol) diacrylate

Table 1 Material viscosity at 4 °C and 25 °C

Material	Viscosity (mPa·s)	
	4 °C	25 °C
+0% PEGDA	23.86	67.39
+3% PEGDA	23.90	79.46
+5% PEGDA	24.35	63.58
+8% PEGDA	24.55	68.94
Water	3.11	1.21
Honey	187,725.19	8,116.18

PEGDA: poly(ethylene glycol) diacrylate

Table 2 Critical gel temperature and storage modulus at 40 °C for different materials

Material	Gelation temperature (°C)	Final G' (Pa)
15% F127DA	22.76	326.09
15% F127DA+3% PEGDA	26.20	271.23
15% F127DA+5% PEGDA	26.76	396.07
15% F127DA+8% PEGDA	28.51	374.40

G': storage modulus; F127DA: polyether F127 diacrylate; PEGDA: poly(ethylene glycol) diacrylate

was significantly better than that printed using pure F127DA (Fig. 4b).

Several factors may have affected the printing accuracy, and these are discussed in depth below. In a previous study, Huh et al. studied two factors (i.e., photoinitiators and UV absorbers) that affected the printing accuracy. They found that the printing accuracy was greatest when the concentration of the photoinitiator LAP was 0.2% (2 g/L) [35]. In this study, we also used LAP as an initiator and lemon yellow as a UV absorber. Specifically, we used 0.25% LAP and selected different concentrations of UV absorbers. It was found that under the same exposure time, layer height, and light intensity, the printing precision of our structure was highest when the UV absorber concentration was 0.1%–0.2% (1–2 g/L) (Fig. S1 in Supplementary Information).

The main factor affecting the printing accuracy was the DMD of the printer itself. We used an EFL-BP8601Pro printer, which has an optical mechanical accuracy of 25 μm. Although precision can reach the micron level, the highest precision of our printing setup reached only 200–300 μm.

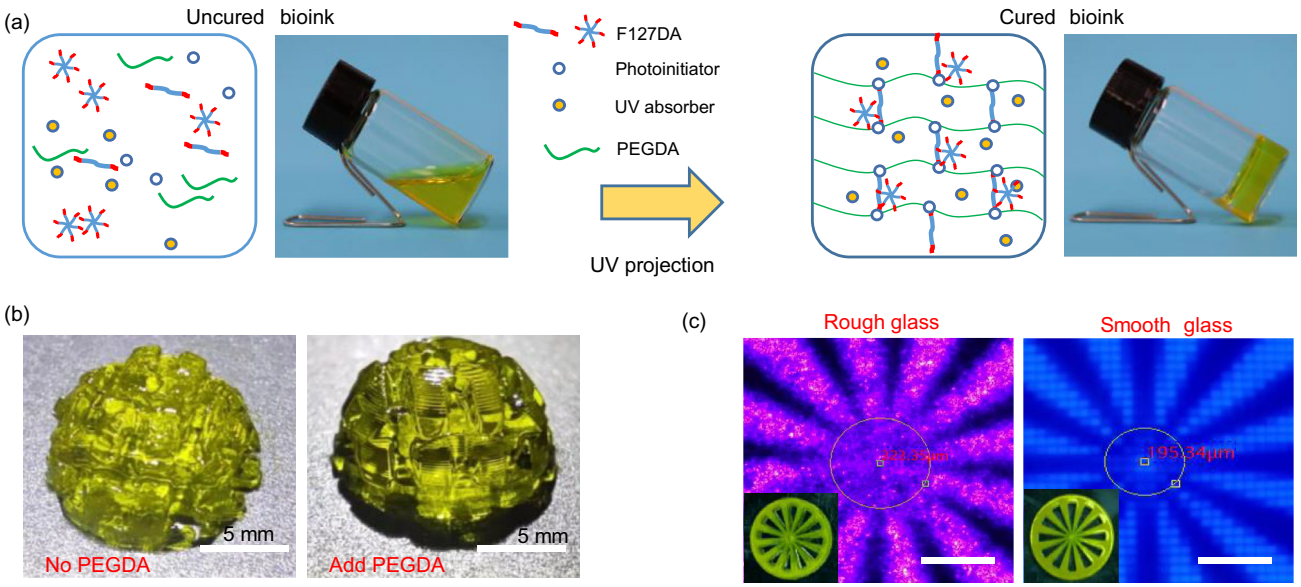

Fig. 4 Factors affecting the printing accuracy. **a** State of the bioink before and after curing. **b** The effect of PEGDA addition on printing accuracy. **c** Photomechanical projection of different light transmitting materials. Observations of the projections of rough and smooth glass on the focal plane using a microscope. The precision of the smooth glass is 200 μm, and that of the rough glass is 300 μm. Scale bar=200 μm. PEGDA: poly(ethylene glycol) diacrylate

Therefore, we tested the light transmission of the material trough (Fig. 4c). To do so, we placed the material trough under a microscope, irradiated it with 405 nm light, and took the image of its projected focal plane. We found that rough and smooth glass projections could both be observed, but the smooth glass pixels could be clearly distinguished while the rough glass pixels were somewhat blurred (Fig. S1 in Supplementary Information). Next, we used a smooth glass trough for printing and found that the printing accuracy still did not reach the desired accuracy for the model design. We then hypothesized that the bioink itself and the model structure affected the printing accuracy. This follows previous research by Shin et al. [36] of Taiwan University, who used digital light processing (DLP) technology to print a high-resolution lattice structure and found that the printed size was larger than that of the imported model.

Biocompatibility

As a biomaterial, F127 shows good biocompatibility for tissue engineering. To evaluate whether F127DA after acryloylation and the addition of PEGDA at different concentrations showed differences in biocompatibility relative to F127, we used HUVEC–material co-cultures to evaluate the material toxicity. Biocompatibility was evaluated using live/dead staining, and cell activity was measured quantitatively via CCK-8 testing and was quantitated by ImageJ (Fig. 5).

Our results showed that the activity of HUVECs decreased with an increasing proportion of PEGDA in F127DA. For example, when PEGDA was added at a concentration of 3% (0.03 g/mL), more than 90% of all cells maintained viability. Moreover, at this concentration, the component material showed good printing performance and compression modulus. Taken together, these findings indicate that the target material has great application potential for tissue engineering.

Implantation

We conducted compression tests on several printed prostheses and two commercial prostheses. The compression modulus of the printed prostheses ((17.12±0.8) kPa) was close to those of the commercial prostheses ((33.00±2.98) kPa) and natural breasts (2–66 kPa) [37, 38]. For all compression tests, the prosthesis was compressed to more than 70% of its original height and showed a good recovery ability by returning to its original form (Fig. 6a).

To better match the properties of breast prostheses to those of human breasts, we further studied the swelling capacity in vitro and degradation behavior in vivo. Figure 6b shows the in vitro swelling test results at different time points. Moreover, the results of our 7-day swelling test showed that the volume and weight of the hydrogel did not change, and the plotted curve showed that the hydrogel maintained good structural stability. Figure 6c shows the appearance of the

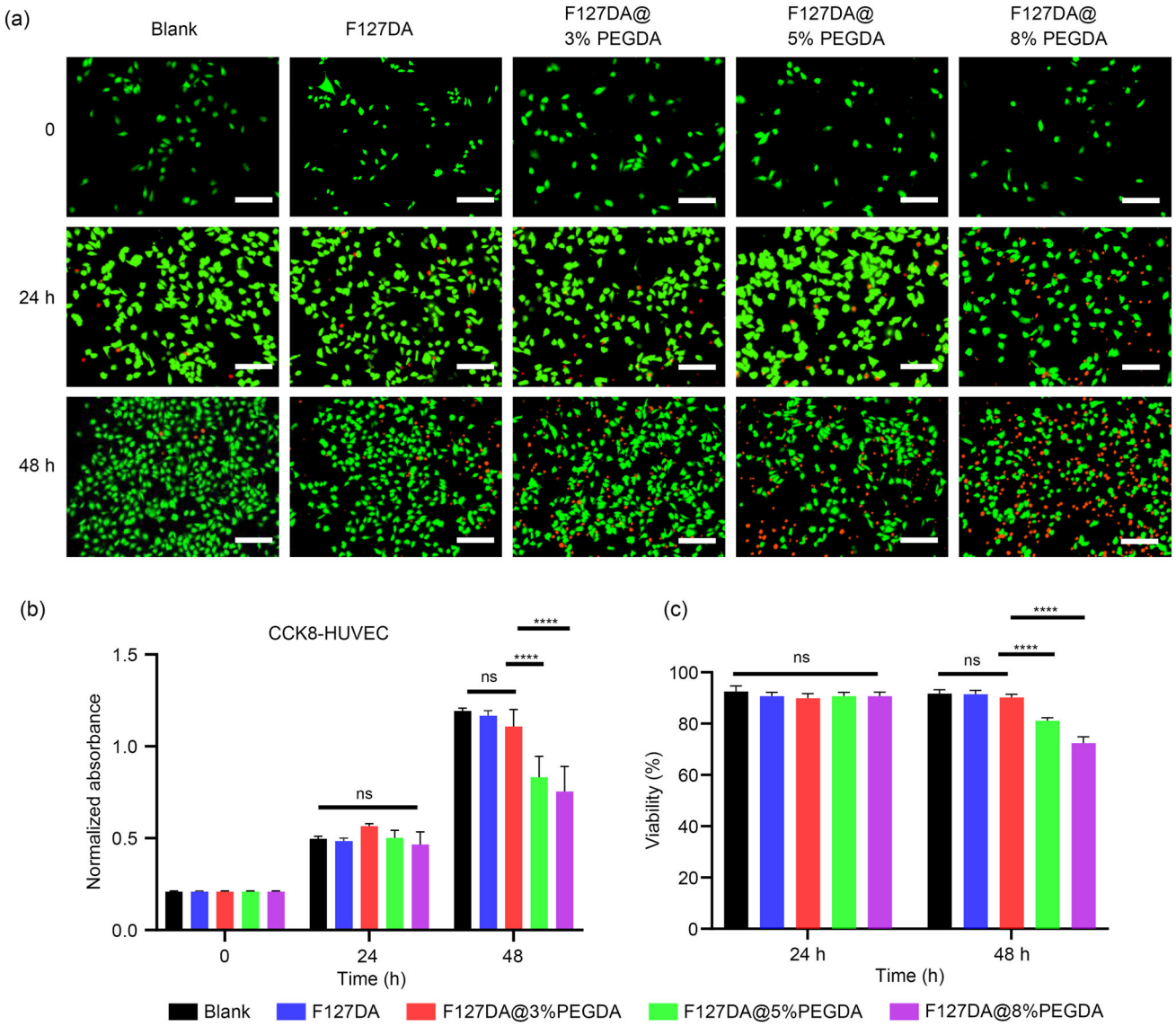

Fig. 5 Biocompatibility analyses of F127, F127DA, and F127DA plus PEGDA. **a** Fluorescent images for live/dead staining show the effect of F127DA, F127DA@3%PEGDA, F127DA@5%PEGDA, and F127DA@8%PEGDA on HUVECs. Scale bar=200 μm. **b** A CCK-8 experiment showed that the material with addition of different concentrations of PEGDA was toxic to cell proliferation. **c** Quantitative counting of living and dead cells via ImageJ. Data are expressed as mean±standard deviation, n=3, $^{****}P<0.0001$. F127DA: polyether F127 diacrylate; PEGDA: poly(ethylene glycol) diacrylate; F127DA@3%PEGDA: F127DA added with 3% PEGDA; F127DA@5%PEGDA: F127DA added with 5% PEGDA; F127DA@8%PEGDA: F127DA added with 8% PEGDA; HUVECs: human umbilical vein endothelial cells; CCK-8: cell counting kit-8

implanted small cuboid after 7, 14, 21, and 28 days; its degradability was then judged by measuring its volume size and weight. These analyses showed that the material did not degrade in vivo over a short time period, which suggests that the material has potential for prosthesis implantation.

Subsequently, we emulsified, centrifuged, and degreased fat samples to obtain SVF-gels (Fig. S2 in Supplementary Information). These SVF-gels were then used to fill the pores of the prosthesis, which was then implanted subcutaneously into nude mice. To observe the fat survival within the implant, we removed implants at different times for HE staining and analysis (Fig. 6d). From a macro perspective, blood vessels could be observed on the surface of the prosthesis by the 14th day, an obvious fat mass was observed by the 28th day, and we found no obvious foreign body reactions. Microscopically, round or multilateral rows of adipose tissue were clearly visible inside the scaffold (Fig. S3 in Supplementary Information).

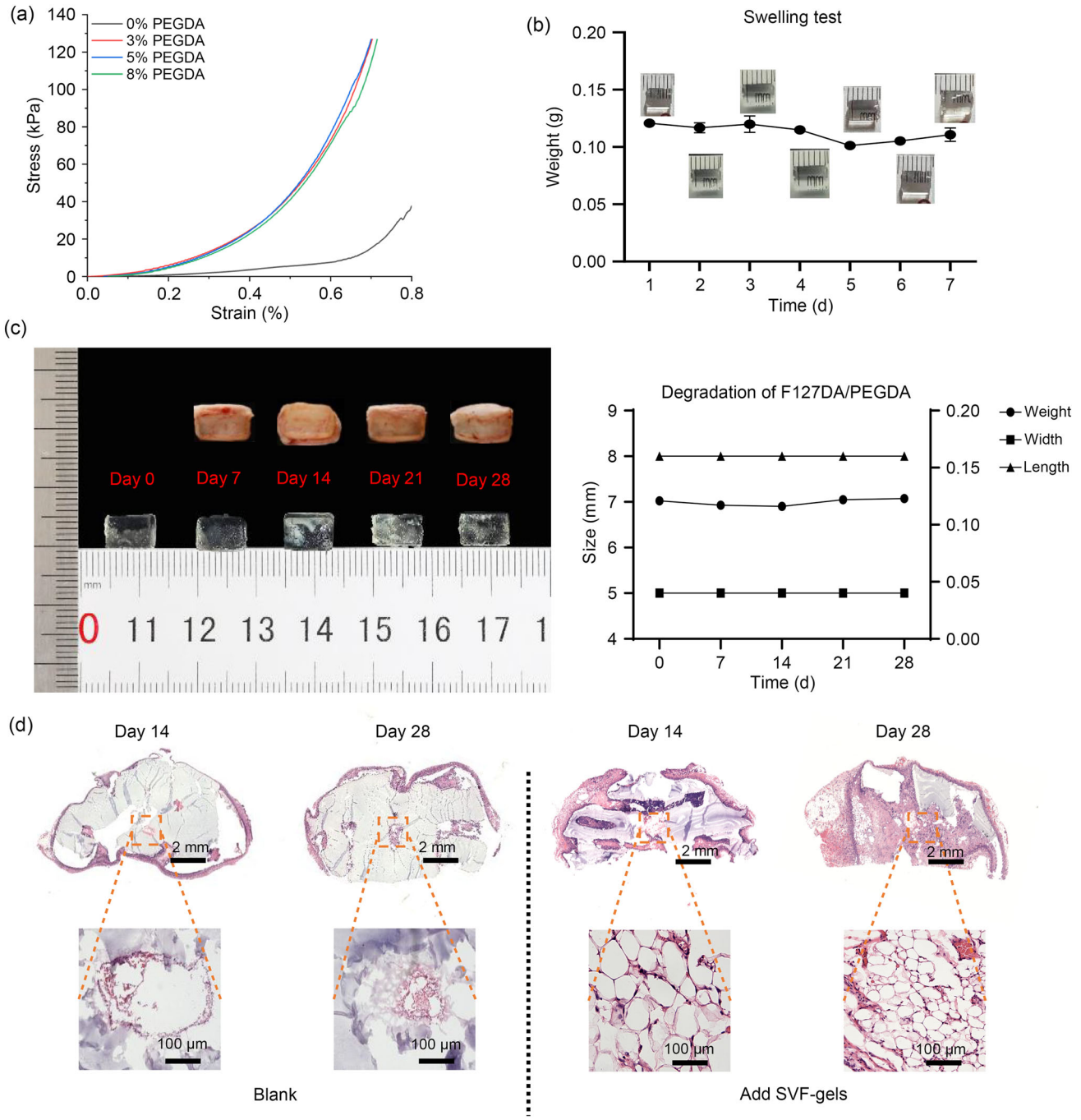

Fig. 6 In vivo and in vitro experiments of the prosthesis biomaterial. **a** Effect of adding different concentrations of PEGDA on the biomaterial compression modulus. **b** In vitro swelling test results. **c** In vivo degradation: a small cuboid of the implant was sampled at different time points, and the volume and weight changes were measured over time. **d** HE staining was used to observe the fat samples derived from the prosthesis on Days 14 and 28 after implantation. PEGDA: poly(ethylene glycol) diacrylate; HE: hematoxylin-eosin

In this study, we developed a porous prosthesis based on PBP technology to achieve breast reconstruction. The biomaterial used for this prosthesis was comprised of F127DA and PEGDA. By adjusting the component ratio of the material and printing parameters, the porous prosthesis was optimized to show relatively good biocompatibility and a compression modulus that was close to that of natural breasts. Next, we used a combination of autologous fat filling and prosthesis reconstruction to achieve breast reconstruction. This can not only ensure the aesthetic appearance of the breast but also solve the problem of "barren" autologous fat. However, this study still has some limitations. First, we did not determine whether the compression modulus of the prosthesis changed after being filled with SVF-gels. Second, we did not conduct quantitative analysis of the components contained in the SVF-gel, nor did we label them. Therefore, we cannot determine whether the implanted fat survived or whether the SVF-gel can promote adipogenic differentiation. In addition, although the same amount of fat was employed in fat transplantation, it was not evenly distributed throughout the prosthesis, and this distribution depends on the operator's experience.

Conclusions

In summary, in this paper we report the development of a new F127DA/PEGDA biological ink and a new method for printing porous prostheses based on the PBP process. Using the synthesis of light-curable F127DA from propylene F127, we carried out a series of tests and found that although F127DA had good printing performance, mechanical properties, and biocompatibility, its gel point was only approximately 23 °C, which led to poor performance in printing of fine structures at room temperature (i.e., approximately 25 °C). Therefore, in this study we added different concentrations of PEGDA to increase the gel point of the bioink system to approximately 26 °C, and then printed porous prosthetic scaffolds with complete pores. Through a biocompatibility test, we selected 15% F127DA and 3% PEGDA as the main components of the printed prosthesis. To use the porous prosthesis for breast reconstruction, we degreased emulsified Coleman fat to obtain SVF-gels, filled the internal pores of the prosthesis, and then implanted the gel-filled prosthesis under the skin of nude mice. The prosthesis was then removed for sectioning and staining, and we found that the fat survived well and achieved the goal of breast reconstruction. Taken together, our results indicate that PBP technology provides a new direction for breast reconstruction, and its high efficiency and high-resolution printing advantages will facilitate improvements in tissue engineering.

Supplementary Information The online version contains supplementary material available at https://doi.org/10.1007/s42242-023-00253-3.

Acknowledgements This work was supported by the National Key Research and Development Program of China (No. 2018YFA0703000), the National Natural Science Foundation of China (Nos. T2121004, 52235007, and 82203602), and Zhejiang Provincial Natural Science Foundation of China under Grant No. LQ22H160020 to JW. This work was also supported by Start-up Funding of Zhejiang Provincial People's Hospital (No. ZRY2021A001 to JW), and Basic Scientific Research Funds of Department of Education of Zhejiang Province (No. KYQN202109 to JW).

Author contributions Conceptualization: YH, PCZ, YDL, and JW. Investigation: PCZ. Some experiments: PCZ, BLW, LW, ZXF, and JH. Writing—original draft: PCZ. Writing & editing: PCZ, BLW, and LW.

Declarations

Conflict of interest YH is an associate editor for *Bio-Design and Manufacturing* and was not involved in the editorial review or the decision to publish this article. The authors declare that they have no conflict of interest.

Ethical approval This experiment was conducted in accordance with the Ethics Committee of Zhejiang Provincial People's Hospital. Adipose tissue used was the fat discarded in plastic surgery liposuction of Zhejiang Provincial People's Hospital. The study protocol obtained informed consent for exemption and was approved by the Ethics Committee of Zhejiang Provincial People's Hospital, Hangzhou, China. The approval code number is QT2022382. The approval code number of Animal Ethical and Welfare is IACUC-A20220054.

References

1. De Santis C, Siegel R, Bandi P et al (2011) Breast cancer statistics. CA Cancer J Clin 61(6):409–418. https://doi.org/10.3322/caac.20134
2. Veronesi U, Boyle P, Goldhirsch A et al (2005) Breast cancer. Lancet 365(9472):1727–1741. https://doi.org/10.1016/S0140-6736(05)66546-4
3. Woolston C (2015) Breast cancer. Nature 527(7578):S120. https://doi.org/10.1038/527S120a
4. Soltanian H, Okada H (2008) Understanding genetic analysis for breast cancer and its implications for plastic surgery. Aesthet Surg J 28(1):85–91. https://doi.org/10.1016/j.asj.2007.10.002
5. Ng SK, Hare RM, Kuang RJ et al (2016) Breast reconstruction post mastectomy: patient satisfaction and decision making. Ann Plast Surg 76(6):640–644. https://doi.org/10.1097/SAP.0000000000000242
6. Strong AL, Cederna PS, Rubin JP et al (2015) The current state of fat grafting: a review of harvesting, processing, and injection techniques. Plast Reconstr Surg 136(4):897–912. https://doi.org/10.1097/PRS.0000000000001590
7. Ellenbogen R (1986) Free autogenous pearl fat grafts in the face—a preliminary report of a rediscovered technique. Ann Plast Surg 16(3):179–194. https://doi.org/10.1097/00000637-198603000-00001
8. Clauser L, Zavan B, Galiè M et al (2019) Autologous fat transfer for facial augmentation: surgery and regeneration. J Craniofac Surg 30(3):682–685. https://doi.org/10.1097/SCS.0000000000005257

9. Nahabedian MY, Patel K (2016) Autologous flap breast reconstruction: surgical algorithm and patient selection. J Surg Oncol 113(8):865–874. https://doi.org/10.1002/jso.24208
10. Patrick CW (2004) Breast tissue engineering. Annu Rev Biomed Eng 6(1):109–130. https://doi.org/10.1146/annurev.bioeng.6.040803.140032
11. Coleman SR, Saboeiro AP (2007) Fat grafting to the breast revisited: safety and efficacy. Plast Reconstr Surg 119(3):775–785. https://doi.org/10.1097/01.prs.0000252001.59162.c9
12. Coleman SR, Lam S, Cohen SR et al (2018) Fat grafting: challenges and debates. Atlas Oral Maxillofac Surg Clin North Am 26(1):81–84. https://doi.org/10.1016/j.cxom.2017.10.006
13. Tonnard P, Verpaele A, Peeters G et al (2013) Nanofat grafting: basic research and clinical applications. Plast Reconstr Surg 132(4):1017–1026. https://doi.org/10.1097/PRS.0b013e31829fe1b0
14. Yu Q, Cai YZ, Huang H et al (2018) Co-transplantation of nanofat enhances neovascularization and fat graft survival in nude mice. Aesthet Surg J 38(6):667–675. https://doi.org/10.1093/asj/sjx211
15. Mineda K, Kuno S, Kato H et al (2014) Chronic inflammation and progressive calcification as a result of fat necrosis: the worst outcome in fat grafting. Plast Reconstr Surg 133(5):1064–1072. https://doi.org/10.1097/PRS.0000000000000097
16. Ye Y, Zou JJ, Tan MJ et al (2021) Phenotypic and cellular characteristics of a stromal vascular fraction/extracellular matrix gel prepared using mechanical shear force on human fat. Front Bioeng Biotechnol 9:638415. https://doi.org/10.3389/fbioe.2021.638415
17. Wolfram D, Rabensteiner E, Grundtman C et al (2012) T regulatory cells and TH17 cells in peri-silicone implant capsular fibrosis. Plast Reconstr Surg 129(2):327e–337e. https://doi.org/10.1097/PRS.0b013e31823aeacf
18. Kadin ME, Morgan J, Xu HY et al (2018) IL-13 is produced by tumor cells in breast implant-associated anaplastic large cell lymphoma: implications for pathogenesis. Hum Pathol 78:54–62. https://doi.org/10.1016/j.humpath.2018.04.007
19. Agrawal R, Kumar A, Mohammed MKA et al (2023) Biomaterial types, properties, medical applications, and other factors: a recent review. J Zhejiang Univ Sci A 23(1):1–16. https://doi.org/10.1631/jzus.A2200403
20. Ramezani H, Zhou LY, Shao L et al (2020) Coaxial 3D bioprinting of organ prototyps from nutrients delivery to vascularization. J Zhejiang Univ Sci A 21(11):859–875. https://doi.org/10.1631/jzus.A2000261
21. Sindi R, Wong YH, Yeong CH et al (2020) Development of patient-specific 3D-printed breast phantom using silicone and peanut oils for magnetic resonance imaging. Quant Imaging Med Surg 10(6):1237–1248
22. Tytgat L, Van Damme L, Ortega Arevalo MDP et al (2019) Extrusion-based 3D printing of photo-crosslinkable gelatin and κ-carrageenan hydrogel blends for adipose tissue regeneration. Int J Biol Macromol 140:929–938. https://doi.org/10.1016/j.ijbiomac.2019.08.124
23. Shi XL, Cheng YX, Wang J et al (2020) 3D printed intelligent scaffold prevents recurrence and distal metastasis of breast cancer. Theranostics 10(23):10652–10664. https://doi.org/10.7150/thno.47933
24. Lee SY, Tae G (2007) Formulation and in vitro characterization of an in situ gelable, photo-polymerizable Pluronic hydrogel suitable for injection. J Controlled Release 119(3):313–319. https://doi.org/10.1016/j.jconrel.2007.03.007
25. Wu CJ, Gaharwar AK, Chan BK et al (2011) Mechanically tough pluronic F127/laponite nanocomposite hydrogels from covalently and physically cross-linked networks. Macromolecules 44(20):8215–8224. https://doi.org/10.1021/ma200562k
26. Sun YN, Gao GR, Du GL et al (2014) Super tough, ultra-stretchable, and thermoresponsive hydrogels with functionalized triblock copolymer micelles as macro-cross-linkers. ACS Macro Lett 3(5):496–500. https://doi.org/10.1021/mz500221j
27. Kim SH, Yeon YK, Lee JM et al (2018) Precisely printable and biocompatible silk fibroin bioink for digital light processing 3D printing. Nat Commun 9(1):1620–1634. https://doi.org/10.1038/s41467-018-03759-y
28. Zhou M, Hou JF, Zhang G et al (2019) Tuning the mechanics of 3D-printed scaffolds by crystal lattice-like structural design for breast tissue engineering. Biofabrication 12(1):015023. https://doi.org/10.1088/1758-5090/ab52ea
29. Sang SB, Cheng R, Cao YY et al (2022) Biocompatible chitosan/polyethylene glycol/multi-walled carbon nanotube composite scaffolds for neural tissue engineering. J Zhejiang Univ Sci B 23(1):58–73. https://doi.org/10.1631/jzus.B2100155
30. Elkhoury K, Morsink M, Tahri Y et al (2021) Synthesis and characterization of C2C12-laden gelatin methacryloyl (GelMA) from marine and mammalian sources. Int J Biol Macromol 183:918–926. https://doi.org/10.1016/j.ijbiomac.2021.05.040
31. Han Y, Yang JL, Zhao WW et al (2021) Biomimetic injectable hydrogel microspheres with enhanced lubrication and controllable drug release for the treatment of osteoarthritis. Bioact Mater 6(10):3596–3607. https://doi.org/10.1016/j.bioactmat.2021.03.022
32. Gay PC, Owens RL (2021) Executive summary: optimal NIV medicare access promotion: a technical expert panel report from the American College of Chest Physicians, the American Association for Respiratory Care, the American Academy of Sleep Medicine, and the American Thoracic Society. Chest 160(5):1808–1821. https://doi.org/10.1016/j.chest.2021.06.083
33. Pohmann R (2011) Physical basics of NMR. In: Schröder L, Faber C (Eds.), In vivo NMR Imaging: Methods and Protocols, Humana Press, Totowa, pp 3–21. https://doi.org/10.1007/978-1-61779-219-9_1
34. Sun YN, Liu S, Du GL et al (2015) Multi-responsive and tough hydrogels based on triblock copolymer micelles as multi-functional macro-crosslinkers. Chem Commun 51(40):8512–8515. https://doi.org/10.1039/c4cc10094h
35. Huh JT, Moon YW, Park J et al (2021) Combinations of photoinitiator and UV absorber for cell-based digital light processing (DLP) bioprinting. Biofabrication 13(3):34103. https://doi.org/10.1088/1758-5090/abfd7a
36. Shin CS, Chang YC (2021) Fabrication and compressive behavior of a micro-lattice composite by high resolution DLP stereolithography. Polymers (Basel) 13(5):785. https://doi.org/10.3390/polym13050785
37. Ramião NG, Martins PS, Rynkevic R et al (2016) Biomechanical properties of breast tissue, a state-of-the-art review. Biomech Model Mechanobiol 15(5):1307–1323. https://doi.org/10.1007/s10237-016-0763-8
38. Gefen A, Dilmoney B (2007) Mechanics of the normal woman's breast. Technol Health Care 15(4):259–271. https://doi.org/10.3233/THC-2007-15404